附件1

浙江工程师学院（浙江大学工程师学院）
同行专家业内评价意见书

姓名： 金巨烽

学号： 22260209

申报工程师职称专业类别（领域）： 材料与化工

浙江工程师学院（浙江大学工程师学院）制

2025年05月26日

填表说明

一、本报告中相关的技术或数据如涉及知识产权保护、军工项目保密等内容，请作脱密处理。

二、请用宋体小四字号撰写本报告，可另行附页或增加页数，A4纸双面打印。

三、表中所涉及的签名都必须用蓝、黑色墨水笔，亲笔签名或签字章，不可以打印代替。

四、同行专家业内评价意见书编号由工程师学院填写，编号规则为：年份4位＋申报工程师职称专业类别(领域)4位+流水号3位，共11位。

一、个人申报

（一）基本情况【围绕《浙江工程师学院（浙江大学工程师学院）工程类专业学位研究生工程师职称评审参考指标》，结合该专业类别(领域)工程师职称评审相关标准，举例说明】

1.对本专业基础理论知识和专业技术知识掌握情况(不少于200字)

1.
完成材料科学核心课程学习，包括《金属学原理与先进合金材料》、《材料加工技术》和《材料现代研究方法与应用实践》等专业课程，课程平均成绩为87，掌握了本专业基础理论知识；

2. 通过了大学英语六级，掌握相关领域专业术语，能熟练阅读、翻译、总结英文资料；

3.
掌握了熔炼炉、轧机、扫描电子显微镜等科研设备的使用，同时掌握origin绘图软件、Thermol-Calch和Jmatpro热力学计算软件以及常用办公软件的使用；

4.
掌握母合金制备、合金变形(开坯及多道次热/冷轧制工艺调控)、热处理制度制定、显微组织分析、失效变形机理分析等核心技术，具备从显微组织观察到宏观性能优化的全流程实验方案制定及研究分析的能力。

2.工程实践的经历(不少于200字)

作为材料工程师在浙江省科创新材料研究院实习一年以上，承担"镍基变形高温合金GH4350组织与拉伸性能研究"的课题。该课题目标是自主研发高性能紧固件用镍基变形合金GH4350，完善该合金熔炼、变形、热处理工艺，实现800℃拉伸性能优化。作为该课题负责人，主导制定合金"成分配比-熔炼-变形-热处理-性能表征-失效分析-
性能优化"全工艺方案，包括：

a)
利用相图计算确定GH4350合金成分配比，利用真空感应和真空自耗双联冶炼自主熔炼合金，利用能谱(EDS)等方式进行成分检测，精确控制合金主要成分并降低有害杂质的含量；

b)
设计变形加工工艺，并制定热处理制度，利用SEM、TEM等设备进行表征，实现合金显微结构调控；

c)
进行合金800℃拉伸性能测试，分析性能数据，利用SEM、TEM等进行表征，并分析失效机理，实现性能优化。

研究成果包括高质量GH4350铸锭冶炼工艺，热轧、冷轧两种板材制备工艺，合金显微组织热处理调控方法，合金800℃拉伸性能失效变形机理，基于变形工艺和热处理工艺的合金性能优化策略，最终合金800℃拉伸性能提升13%，达到同类合金先进水平，并完成了2篇英文论文，已经分别被录用和发表。

3.在实际工作中综合运用所学知识解决复杂工程问题的案例（不少于1000字）

航空紧固件是镍基变形高温合金体系的重要应用方向之一，此类紧固件承担着航空发动机热端部件连接的关键功能，是重要的通用基础产品，被誉为"工业之米"。航空发动机推重比与进气温度的持续提升，对热端连接紧固件的耐温性能提出了更高要求。为满足新一代航空发动机极端服役环境的需求，开发耐高温性能更优的紧固件材料已成为当前研究重点。GH4350合金作为典型紧固件用镍基变形高温合金，最高使用温度达750℃，该合金兼具优异的拉伸、抗疲劳、持久和蠕变性能，同时在高温环境下仍保持低热膨胀

系数、低缺口敏感性及良好耐蚀性。基于其综合性能优势，GH4350有潜力进一步提升使用温度至800℃。该合金主要通过细晶强化、固溶强化以及γ′相沉淀强化获得高强度，但在γ′相析出的同时也会析出少量η相，该相在热处理过程中随"温度-时间"参数演变，对合金性能具有双重影响，其形貌分布既可阻碍位错运动提升强度，也可能成为裂纹萌生源。拉伸性能是变形高温合金关键的力学性能之一，对于紧固件的安全服役具有重要意义，因此需要深入研究GH4350在800℃拉伸性能与显微组织的关系。

目前缺乏协同调控γ′相和η相析出分布特征以及η相与800℃拉伸变形机理的关联关系的研究。针对上述问题，我和研究团队基于工程实践上的便捷性，提出多步时效热处理策略来解决η相与γ′相协同定量调控的难题。首先基于Thermo-Calc软件相图计算获得γ′相与η相的临界固溶温度，结合JMatPro软件时效动力学模拟制定了680℃~1000℃多温区时效热处理制度。针对文献中普遍存在的η相析出行为定量数据缺失问题，我和研究团队创新性地建立了四维特征参数体系：（1）平均长度表征相尺寸演化；（2）面积分数反映析出总量；（3）长度分布半峰宽描述析出均匀性；（4）峰值长度确定主要析出长度。

通过定量分析发现：第一，η相析出呈现显著的三阶段演变规律。当时效温度低于810℃时，η相主要在晶界以短棒状形态析出，其特征参数均保持较低水平（平均长度<1μm、面积分数<0.3%、峰值长度<0.7μm、半峰宽<1μm），且尺寸分布均匀；当温度升至840℃~900℃区间，η相仍以晶界析出为主，但形貌转变为板片状，特征参数显著增加（平均长度1μm~3.5μm、面积分数0.5%~2%、峰值长度1μm~2μm），同时半峰宽增至约2μm，尺寸均匀性明显下降；当温度超过900℃，η相析出模式转变为晶内析出主导，并在高温区逐步减少。第二，γ′相析出呈现两段式规律：在810℃以下，随着时效温度升高，晶内硬度由350HV持续增至410HV，表明γ′相析出量逐步增加；而当时效温度超过810℃后，晶内硬度下降至250HV，反映γ′相析出受到抑制。

基于上述规律，我和研究团队提出时效工艺设计准则：首先通过一步时效（低温或高温）控制η相的晶界析出形貌（短棒状或板片状），随后通过二步低温时效促进γ′相析出。该研究建立的量化特征参数体系为时效热处理工艺的精确设计提供了科学依据。具体而言，我和研究团队设计了两种二步时效热处理制度：H1热处理（780℃/4h+750℃/4h）和H2热处理（870℃/4h+750℃/4h）。H1热处理使得η相在晶界呈短棒状析出，H2热处理使得η相在晶界呈板片状析出，然后对这两种样品进行了800℃拉伸性能测试，并利用扫描电子显微镜和透射电子显微镜分析并比较了不同η相析出分布特征的样品在800℃拉伸条件下的变形行为。结果显示，短棒状η相附近变形集中，易萌生裂纹，同时其沿晶界近似平行分布并形成γ′相贫乏区，导致局部软化，不能阻碍裂纹扩展，因此利于裂纹连接并沿晶界扩展，最终导致沿晶断裂的发生；板片状η相之间形成γ′相贫乏区，但其与晶界呈一定角度，能够阻碍裂纹扩展，导致裂纹需要更高的应力克服板片状η相的阻碍才能继续扩展，最终使得合金的抗拉强度提升13%。

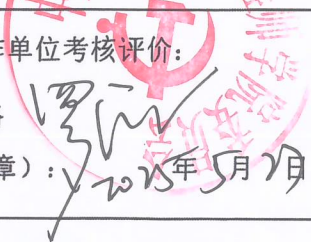在本案例中，我综合利用各种材料学知识，结合统计分析的方法，解决了η相与γ′相定量协同调控的难题，并建立了η相析出分布特征与800℃拉伸性能的关联机制。研究结果可为该合金在800℃服役条件下的高温拉伸性能优化提供组织设计指导：引入板片状η相提升强度。通过该工程实践，我掌握了熔炼设备、变形加工设备以及显微组

织表征设备的使用，参加了一次学术会议并发表两篇论文，具备一定的实验设计能力和科学创新能力。

（二）取得的业绩（代表作）【限填3项，须提交证明原件（包括发表的论文、出版的著作、专利证书、获奖证书、科技项目立项文件或合同、企业证明等）供核实，并提供复印件一份】

1.
公开成果代表作【论文发表、专利成果、软件著作权、标准规范与行业工法制定、著作编写、科技成果获奖、学位论文等】

成果名称	成果类别 [含论文、授权专利（含发明专利申请）、软件著作权、标准、工法、著作、获奖、学位论文等]	发表时间/授权或申请时间等	刊物名称/专利授权或申请号等	本人排名/总人数	备注
Review on microstructure and strength-enhancing characteristics of superalloy GH4350	一级期刊	2024年11月12日	稀有金属材料与工程	1/6	SCI期刊收录
Morphology control of η phase in enhancing high-temperature tensile property of superalloy GH4350	一级期刊	2025年04月20日	Journal of Alloys and Compounds	1/11	SCI期刊收录
镍基变形高温合金GH4350组织和拉伸性能研究	学位论文送审专家评阅结果全优	2025年04月18日		1/1	学位论文

2.其他代表作【主持或参与的课题研究项目、科技成果应用转化推广、企业技术难题解决方案、自主研发设计的产品或样机、技术报告、设计图纸、软课题研究报告、可行性研究报告、规划设计方案、施工或调试报告、工程实验、技术培训教材、推动行业发展中发挥的作用及取得的经济社会效益等】

（三）在校期间课程、专业实践训练及学位论文相关情况	
课程成绩情况	按课程学分核算的平均成绩： 87 分
专业实践训练时间及考核情况(具有三年及以上工作经历的不作要求)	累计时间： 1.1 年（要求1年及以上） 考核成绩： 85 分
本人承诺	

个人声明：本人上述所填资料均为真实有效，如有虚假，愿承担一切责任，特此声明！

申报人签名：金巨烽

二、日常表现考核评价及申报材料审核公示结果

日常表现 考核评价	非定向生由德育导师考核评价、定向生由所在工作单位考核评价： ☑优秀　　☐良好　　☐合格　　☐不合格 德育导师/定向生所在工作单位分管领导签字（公章）：　2025年5月7日
申报材料 审核公示	根据评审条件，工程师学院已对申报人员进行材料审核（学位课程成绩、专业实践训练时间及考核、学位论文、代表作等情况），并将符合要求的申报材料在学院网站公示不少于5个工作日，具体公示结果如下： 　☐通过　　　☐不通过（具体原因：　　　　　　　　　　） 工程师学院教学管理办公室审核签字（公章）：　　　　年　月　日

浙 江 大 学 研 究 生 院

攻读硕士学位研究生成绩表

| 学号：22260209 | 姓名：金巨烽 | | 性别：男 | 学院：工程师学院 | | 专业：材料与化工 | | | 学制：2.5年 |

| 毕业时最低应获：24.0学分 | | 已获得：26.0学分 | | | 入学年月：2022-09 | | | 毕业年月： | |

| 学位证书号： | | | 毕业证书号： | | | 授予学位： | | | |

学习时间	课程名称	备注	学分	成绩	课程性质	学习时间	课程名称	备注	学分	成绩	课程性质
2022-2023学年秋季学期	新时代中国特色社会主义理论与实践		2.0	89	公共学位课	2022-2023学年冬季学期	材料现代研究方法与应用实践		2.0	91	专业学位课
2022-2023学年秋季学期	工程技术创新前沿		1.5	86	专业学位课	2022-2023学年秋冬学期	高阶工程认知实践		3.0	91	专业学位课
2022-2023学年秋季学期	金属学原理与先进合金材料		2.0	87	专业学位课	2022-2023学年冬季学期	产业技术发展前沿		1.5	89	专业学位课
2022-2023学年冬季学期	材料加工技术		2.0	88	专业选修课	2022-2023学年夏季学期	研究生英语基础技能		1.0	免修	公共学位课
2022-2023学年秋冬学期	工程伦理		2.0	96	公共学位课	2022-2023学年夏季学期	自然辩证法概论		1.0	88	公共学位课
2022-2023学年秋冬学期	研究生论文写作指导		1.0	88	专业学位课	2022-2023学年夏季学期	研究生英语		2.0	免修	公共学位课
2022-2023学年秋冬学期	数据分析的概率统计基础		3.0	74	专业选修课		硕士生读书报告		2.0	通过	

说明：1.研究生课程按三种方法计分：百分制，两级制（通过、不通过），五级制（优、良、中、

　　　　及格、不及格）。

　　　2.备注中"*"表示重修课程。

学院成绩校核章：

成绩校核人：张梦依

打印日期：2025-06-03

《稀有金属材料与工程》中英文版论文录用通知单

尊敬的金巨烽, 赵新宝, 赵倩敏, 岳全召, 谷月峰, 张泽先生/女士：您好！

您的论文 《镍基变形高温合金 GH4350 的微观结构特征综述》(编号：20240656)经审稿决定录用。请不要再投其他期刊。

《稀有金属材料与工程》、《Rare Metal Materials and Engineering》是 SCI 收录的中国科技期刊卓越行动计划集群化试点项目期刊。

关于论文保密审查的声明：本刊要求凡是涉密论文需要预先进行保密审查，作者及所在单位对失密承担法律责任，编辑部不承担连带责任。

该论文已被该期刊录用，该期刊是 SCI 收录期刊

赵新宝

2025. 3. 8

Journal	Publisher	ISSN	eISSN	Country	Category		
RAIRO-THEORETICAL INFORMATICS AND APPLICATIONS	EDP SCIENCES	0988-3754	1290-385X	FRANCE	COMPUTER SCIENCE, INFORMATION	0.319	0.385
RAMANUJAN JOURNAL	SPRINGER	1382-4090	1572-9303	NETHERLANDS	MATHEMATICS; Q3/	0.563	0.635
Random Matrices-Theory and Applications	WORLD SCI	2010-3263	2010-3271	SINGAPORE			
RANDOM STRUCTURES & ALGORITHMS	WILEY-	1042-9832	1098-2418	UNITED STATES	MATHEMATICS; Q1/MATHEMATICS,	1.011	1.086
Range Management and Agroforestry	RANGE	0971-2070		INDIA	AGRONOMY; Q4/	0.391	0.302
Rangeland Ecology & Management	SOC RANGE	1550-7424	1551-5028	UNITED STATES	ENVIRONMENTAL SCIENCES;	1.349	1.696
RANGELAND JOURNAL	CSIRO	1036-9872	1834-7541	AUSTRALIA	ECOLOGY; Q3/	1.194	1.281
RAPID COMMUNICATIONS IN MASS SPECTROMETRY	WILEY-	0951-4198	1097-0231	ENGLAND	SPECTROSCOPY; Q2/CHEMISTRY,	2.226	2.335
RAPID PROTOTYPING JOURNAL	EMERALD	1355-2546	1758-7670	ENGLAND	ENGINEERING, MECHANICAL;	1.352	1.851
RARE METAL MATERIALS AND ENGINEERING	NORTHWEST	1002-185X	1002-185X	PEOPLES R CHINA	METALLURGY & METALLURGICAL	0.236	0.287
RARE METALS	NONFERROUS	1001-0521	1867-7185	PEOPLES R CHINA	METALLURGY & METALLURGICAL	0.957	0.792
Reaction Kinetics Mechanisms and Catalysis	SPRINGER	1878-5190	1878-5204	HUNGARY	CHEMISTRY, PHYSICAL; Q3/	1.265	1.131
REACTIVE & FUNCTIONAL POLYMERS	ELSEVIER	1381-5148	1873-166X	NETHERLANDS	ENGINEERING, CHEMICAL;	2.725	2.706
REAL-TIME SYSTEMS	SPRINGER	0922-6443	1573-1383	NETHERLANDS	COMPUTER SCIENCE, THEORY &	0.738	0.943
Recent Patents on Anti-Cancer Drug Discovery	BENTHAM	1574-8928	2212-3970	U ARAB EMIRATES	PHARMACOLOGY & PHARMACY;	3.533	2.638
Recent Patents on Nanotechnology	BENTHAM	1872-2105	2212-4020	U ARAB EMIRATES	PHYSICS, APPLIED; Q3/MATERIALS	1.576	1.446
Recht & Psychiatrie	PSYCHIATRIE	0724-2247		GERMANY	PSYCHIATRY; Q4/	0.350	0.357
Rechtsmedizin	SPRINGER	0937-9819	1434-5196	GERMANY	MEDICINE, LEGAL; Q4/	0.324	0.359
Records of Natural Products	ACG	1307-6167		TURKEY	PLANT SCIENCES; Q3/CHEMISTRY,	0.765	1.217
RECORDS OF THE AUSTRALIAN MUSEUM	AUSTRALIAN	0067-1975	0067-1975	AUSTRALIA	ZOOLOGY; Q3/	0.714	0.774
Records of the Australian Museum Supplement	AUSTRALIAN	0812-7387		AUSTRALIA			
REDIA-GIORNALE DI ZOOLOGIA	CRA-	0370-4327		ITALY	ZOOLOGY; Q4/	0.615	0.511
Redox Biology	ELSEVIER	2213-2317	2213-2317	NETHERLANDS	BIOCHEMISTRY & MOLECULAR	6.235	6.235

ARTICLE

Review on microstructure and strength-enhancing characteristics of superalloy GH4350

Jin   Jufeng[1, 2],   Zhao   Xinbao [1, 3],   Zhao   Qianmin [1, 2],   Yue Quanzhao [1],   Gu Yuefeng [1, 3],   Zhang Ze [1, 3]

[1] Institute of Superalloys Science and Technology, School of Materials Science and Engineering, Zhejiang University, Hangzhou 310027, Zhejiang, China; [2] Polytechnic Institute, Zhejiang University, Hangzhou 310027, Zhejiang, China; [3] State Key Laboratory of Silicon and Advanced Semiconductor Materials, Zhejiang University, Hangzhou 310027, Zhejiang, China

Abstract: GH4350, or AEREX 350, is a Ni-based wrought superalloy developed for high-performance fasteners operating up to 750°C. It is valued for its high tensile strength, fatigue resistance, stress rupture and relaxation resistance, corrosion resistance, low thermal expansion, and notch sensitivity. GH4350's strength is largely derived from the incorporation of solid solution strengthening elements and the precipitation of γ' phases, along with a minor presence of η phases. However, the alloy's microstructure is sensitive to heat treatment, as γ' phases can transform into η phases under certain conditions, potentially reducing its performance. This transformation is influenced by specific heat treatment parameters, including temperature and time. This review provides an overview of GH4350's chemical composition characteristics, heat treatment strategies and strength-enhancing characteristics, aiming to deepen understanding of the factors behind its remarkable high temperature properties and to guide the development of new alloys or enhancements to boost its temperature capabilities.

Key words: fastener wrought superalloy GH4350; high temperature strength; chemical composition; heat treatment; η phase

High-temperature alloy materials are extensively utilized in sectors such as aerospace, energy, and metallurgy due to their capacity to retain superior mechanical properties and structural stability under extreme thermal conditions, where conventional materials would fail due to oxidation, creep, and fatigue[1–4]. Typical high-temperature alloy materials include Ni-based superalloys, Co- based superalloys, Al- and Cr-based high-temperature alloys and Pt–Al high-temperature alloys[2,5–9]. The demands of the modern aerospace industry, particularly for aero engines, require enhanced thrust-to-weight ratios and greater fuel efficiency at elevated temperatures, thereby necessitating the development of increasingly advanced high-temperature alloy materials[1,2].

Ni-based wrought superalloys are a class of advanced high-temperature alloy materials that exhibit remarkable high temperature properties including resistance to oxidation, fatigue, and creep, and are extensively utilized in diverse industrial sectors, including aerospace, energy, and marine shipping[5–8].

Fasteners, which are used extensively in the aerospace industry, represent a crucial category of Ni-based wrought superalloys. Their primary function is to join multiple separate components into a single unit, making fasteners an indispensable element in modern industry[10].

GH4350 stands out as a high temperature Ni-based wrought superalloy used in fasteners due to its ability to withstand service temperatures of up to 750 °C[11–13]. Consequently, it must exhibit high tensile and yield strength, along with strong resistance to fatigue, stress rupture, and stress relaxation[14–17]. Additionally, corrosion resistance, low thermal expansion and notch sensitivity are critical factors in fastener applications, particularly at elevated temperatures[15,18]. The production of high-quality superalloy ingots is crucial for achieving the remarkable properties required for such demanding applications. Single-melting techniques such as vacuum induction melting (VIM), vacuum arc remelting (VAR) and electro slag remelting (ESR) are utilized to produce high-quality superalloy ingots

with fewer oxides, such as Al_2O_3 particles[2,8]. To further enhance ingot quality, particularly by reducing inclusions, the duplex-melting processes (e.g., VIM+VAR, VIM+ESR) or triple-melting (VIM+VAR+ESR) processes are employed in the melting of GH4350 master ingots[8,12,19].

Following alloy smelting, the microstructure is refined through a combination of cold and hot working techniques along with heat treatment, which are designed based on the chemical composition and microstructure characteristics, to further improve the properties of the alloy[19]. Previous research has confirmed that in GH4350, the addition of Co, W and Mo contributes to solid solution strengthening in the face-centered cubic (FCC) γ phase while the addition of Al, Ti, Nb and Ta forms γ′ phase which is distributed throughout the γ phase matrix for precipitation strengthening[12,13,18,20,21]. In addition to the γ′ phase, the formation of the hexagonal close-packed (HCP) η phase is notable. This phase develops during heat treatments and is sensitive to temperature and time[21,22]. Understanding the morphology and distribution of η phase is pivotal, as these factors can determine whether its presence is beneficial or detrimental to the alloy's properties[23–27].

This review takes a detailed examination of the chemical composition of GH4350 and various heat treatments, characterized by different microstructures, such as the distribution of γ′ and η phases. It aims to offer valuable insights for optimizing chemical composition and enhancing the existing properties of GH4350 with the goal of further increasing its service temperatures.

1 Chemical compositions and phase constitutions

1.1 The chemical compositions of alloy GH4350

The microstructures of several commonly used Ni-based wrought superalloys for fasteners are summarized in Fig. 1. GH4350, with a service temperature of 750 °C, is derived from the Co-based superalloys MP35N and MP159[12,28]. As illustrated in Fig. 1(a), the γ′ phases are spherical, with an average diameter of 38 nm, and are uniformly distributed throughout the γ matrix[15]. Additionally, plate-like or needle-like η phases predominantly precipitate at grain boundaries, with a smaller fraction of finer η phases forming within the grains[14,15]. In contrast, Alloy 718, as depicted in Fig. 1(b) and (c), is primarily strengthened by γ″ phases, with a minor presence of spherical γ′ phases[14]. Also, short rod-like δ phases and a small amount of blocky MC carbides are presented on grain boundaries[14]. Alloy 718 Plus, shown in Fig. 1(d), is mainly strengthened by γ′ phases, accompanied by minor precipitations of η or δ phases[29]. Furthermore, as illustrated in Fig. 1(e), Waspaloy alloy exhibits a bimodal distribution of γ′ phases, comprising spherical primary γ′ phases and secondary γ′ phases within the matrix, with carbides forming along grain boundaries as a result of heat treatments[14]. A similar distribution of γ′ phases is observed in GH4698, as shown in Fig. 1(f)[30].

These microstructure differences stem from differences in chemical composition as listed in Table 1. GH4350 contains solid solution strengthening elements like W and Mo, as well as precipitation strengthening elements Al and Ti, leading to the precipitations of γ′ phase and η phase. Furthermore, GH4350 adds Ta to improve its mechanical properties. Some reports that the volume fraction of the γ′ phase of the alloy samples aged at 850 °C for 4 h is approximately 18 %[13]. Obviously, GH4350 differs from other wrought Ni-based superalloys in elemental compositions. Alloy 718 adds more Nb and less (Al+Ti), which leads to precipitations of more γ″ phases and less γ′ phases[31–34]. The volume fraction of γ″ phase in a wrought alloy 718 is reported nearly 3 times higher than that of the γ′ phase, estimated at 17.8 % and 6.5 %, respectively. However, at temperatures above 650 °C, the γ″ phase transforms into the less desirable δ phase, which negatively impacts alloy performance. Alloy 718 Plus addresses this issue by increasing Al and Ti content and adjusting the Al/Ti ratio[35]. This modification promotes γ′ phase precipitation, along with a small amount of η or δ phase and raises the service temperature by 55°C [6,29,36,37]. Similar to GH4350, optimized additions of Co and W aim to enhance mechanical properties, thermal stability, and stress rupture properties through solid solution strengthening[29,35].

Increasing the volume fraction of the γ′ phase in superalloys like alloy 718Plus can enhance their service temperature, however, good processing characteristics are also crucial in wrought superalloys alongside high temperature performance. As shown in Table 1, Waspaloy, lacking Nb, contains three times more Ti than alloy 718Plus, totaling about 5 wt% (Al+Ti), resulting in a γ′ phase volume fraction of around 30 % and enables it to withstand temperatures up to 750 °C, higher than alloy 718Plus[38–41]. But its processing properties are less favorable compared to alloy 718Plus due to the higher volume fraction of γ′ phase and faster γ′ phase precipitation[35]. A similar issue is likely present in GH4698 which has about 4.5 wt% (Al+Ti) content despite its significant γ′ phase volume fraction that improves service temperature, it may also face challenges in processing characteristics. The relatively lower (Al+Ti) content in GH4350 compared to other alloys listed in Table 1 may be intended to moderate γ′ phase formation, preventing an excessive increase in deformation resistance, and thus allowing GH4350 to maintain a favorable combination of strength and deformability.

1.1.1 Solid solution strengthening elements

The Ni-based γ phase of the matrix characterized by a FCC crystal structure can dissolves some alloying elements primarily including Co, Cr, Mo, and W. These solute elements interact with matrix and cause lattice misfit and modulus misfit which will impede dislocation movement and enhance the performance of superalloys[42,43].

The solid solution strengthening effect of each element i ($\Delta\sigma_{SSi}$) has been quantitatively evaluated in Ni-X_i binary alloy systems by many researchers and they believe that the solid solution strengthening effect results from the interaction of solute

atoms with dislocations[43–50]. On this basis, $\Delta\sigma_{SSSi}$ can be calculated by[51,52]:

$$\Delta\sigma_{SSSi}=K_i c_i^{1/2} \qquad (1)$$

where K_i and c_i are strengthening constant and atomic percentage of solute element i, respectively.

In the case of multi-component Ni-based superalloys, the total solid solution strengthening effects ($\Delta\sigma_{SSS}$) can be assessed by the method of Gypen and Deruyttere[53]:

$$\Delta\sigma_{SSS}=\left(\sum_i \Delta\sigma_{SSSi}^2\right)^{1/2} \qquad (2)$$

Combining Eq. (1) and Eq. (2), the $\Delta\sigma_{SSS}$ is expressed as:

$$\Delta\sigma_{SSS}=\left(\sum_i K_i^2 c_i\right)^{1/2} \qquad (3)$$
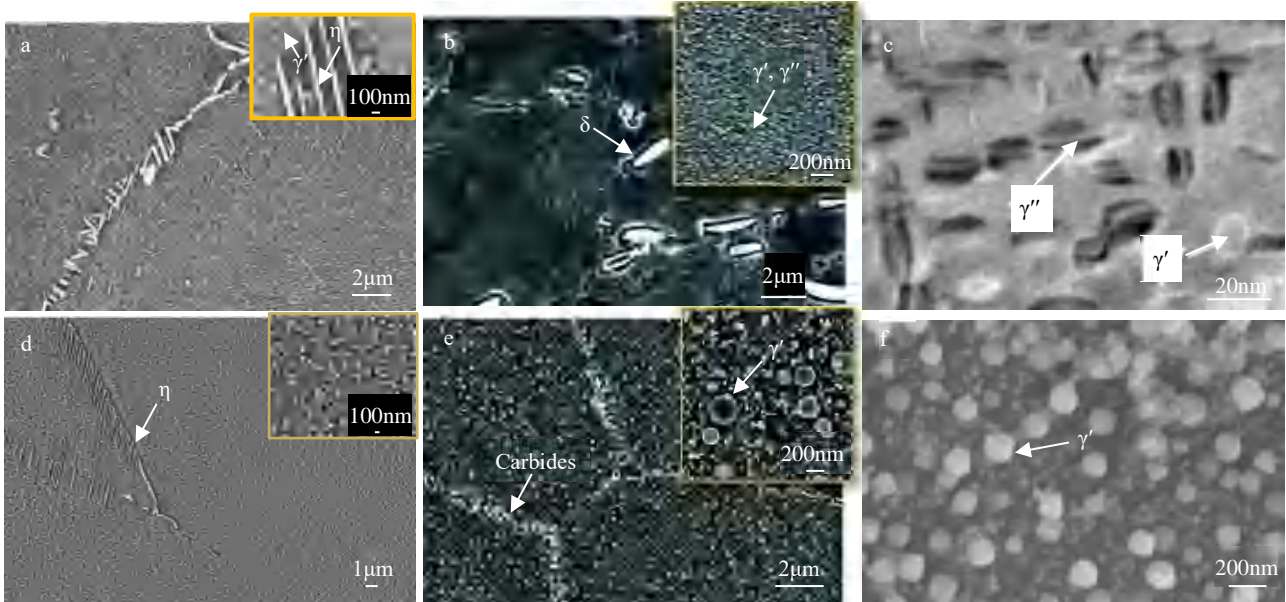
Fig. 1 Typical microstructures of Ni-based wrought superalloys. (a) Microstructure of GH4350. (b) and (c) Microstructure of alloy 718. (d) Microstructure of alloy 718Plus. (e) Microstructure of Waspaloy alloy. (f) Microstructure of GH4698. (adapted from Refs.[14,15,29,30,54])

Table 1 Chemical compositions of typical Ni-based wrought superalloys for fasteners(wt%)[22,35,41,55]

Ni-based	Ni	Cr	Co	Mo	W	Nb	Al	Ti	Fe	C	P+B	Ta
718	Bal.	19	/	3.0	/	5.15	0.6	0.9	18.5	0.04	0.01	/
718 Plus	Bal.	18.0	9.1	2.7	1.0	5.4	1.45	0.75	9.5	0.020	0.011	/
Waspaloy	Bal.	19.0	13.5	4.0	/	/	1.9	3.0	/	0.07	0.005	/
GH4698	Bal.	14.68	/	3.05	/	2.09	1.68	2.7	0.47	0.048	/	/
GH4350	Bal.	17	25	3	2	1.2	1.0	2.2	/	$\leqq 0.025$	$\leqq 0.025$	4

K_i can be determined by analyzing 0.2 % flow stress experimental data on the solution strengthening of Ni-X_i binary alloys[51,52]. The results are shown in Fig. 2. Elements with larger K_i generally indicate a greater potential for solid solution strengthening such as Mo, W, Ta and Nb. It is reasonable for major precipitation strengthening element Al to obtain a low strengthening constant.

The addition of a large amount of Co is one distinguishing feature of GH4350 compared to other Ni-based wrought superalloys. As shown in Fig. 2, adding Co atoms contribute to solid solution strengthening. In addition, as a matrix element, Co facilitates the transformation of part of the γ matrix from FCC to HCP which induces a strengthening effect by the presence of two distinct crystal structures creating a barrier to dislocation motion during cold working[18,56,57]. Another important impact of Co addition is its influence on stacking defects. Co reduces stacking fault energy which inhibits the cross-slip motion of dislocations, thereby suppressing dislocation annihilation and improving the ability of twinning, leading to enhanced strain hardening capability of the superalloys[58].

In addition, firstly, solid solution strengthening elements are effective only if they successfully enter the matrix. Therefore, these elements must preferentially partition to the γ matrix. Alloying elements can be categorized into two groups based on their partitioning coefficient $k_i^{\gamma'}$, as defined below[59]:

$$k_i^{\gamma'}=\frac{c_i^{\gamma'}}{c_i^{\gamma}} \qquad (4)$$

where $c_i^{\gamma'}$ and c_i^{γ} represent the atomic fractions of element i in the γ′ and γ phases, respectively. Elements such as Co, Cr, Mo, and W are typically enriched in the γ phase (with k<1), whereas elements like Al, Ti, and Ta tend to be enriched in the γ′ phase.

(with k>1)[59,60].

Secondly, these solid solution strengthening elements must form a stable solid solution in the γ matrix, which can continuously hinder dislocation movement. To maintain their strengthening effect, especially at high temperatures, these elements should not diffuse extensively. This requires a low diffusion rate in the matrix. The diffusion coefficient of element i in the γ phase at temperature T, denoted as $D_T^{i,\,Ni}$, is given as follows[61–64]:

$$D_T^{i,\,Ni}=D_0^{i,\,Ni}\exp\left(\frac{-Q^{i,Ni}}{RT}\right) \quad (5)$$

where $D_0^{i,\,Ni}$ and $Q^{i,Ni}$ are the pre-exponential factor and the activation energy for interdiffusion of element i in Ni, respectively.

For example, when calculating the diffusion coefficients of the elements at 800°C, the results in Table 2 demonstrate that the diffusion coefficients vary significantly among the elements. Specifically, the diffusion coefficients of Nb, Ta, Ti, and Al are higher, while those of Cr, Co, Mo, and W are lower. As a result, the latter elements diffuse more slowly at high temperatures, thereby better maintaining the solid solution strengthening effect.

Table 2 diffusion coefficient calculation of typical elements at T= 800 °C[61,62,65,66]

element	$D_0^{i,\,Ni}$ (m²/s)	$Q^{i,Ni}$(kJ/mol)	$D_{T=800°C}^{i,\,Ni}$(m²/s)
Cr	5.2×10⁻⁴	289	4.45×10⁻¹⁸
Co	1.8×10⁻⁴	282	3.38×10⁻¹⁸
Mo	1.15×10⁻⁴	281	2.41×10⁻¹⁸
W	8.6×10⁻⁶	264	1.21×10⁻¹⁸
Nb	8.8×10⁻⁵	257	2.72×10⁻¹⁷
Ta	2×10⁻⁵	251	1.21×10⁻¹⁷
Ti	4.1×10⁻⁴	275	1.69×10⁻¹⁷
Al	4.3×10⁻⁴	272	2.48×10⁻¹⁷

In addition to the incorporation of Co, the GH4350 alloy also contains W and Mo, with a combined total mass fraction of 5%. Both W and Mo exhibit relatively high solid solution strengthening constants, indicating their significant contribution to the solid solution strengthening of the alloy[67]. These elements primarily partition to the γ matrix phase, and their diffusion coefficients at high temperatures are relatively low, which minimizes their tendency to diffuse out of the matrix. As a result, they effectively maintain the solid solution strengthening effect, thereby significantly enhancing the alloy's strength at elevated temperatures.

1.1.2 Precipitation strengthening elements

Al, Ti and Nb are typical γ′ phase formers and γ′ phase remains stable at high temperatures, effectively hindering dislocation motion. An increase in Al, Ti and Nb content increases the γ′ phase volume fraction, which further enhance the alloy's strength. GH4350 contains a combined weight percentage of 4.5 % of Al, Ti and Nb which signifies a significant potential for precipitation strengthening within the alloy.

In addition to Al, Ti and Nb, Ta also plays a vital role in strengthening the γ′ phase and represents a notable difference in the composition of GH4350 compared to other Ni-based wrought superalloys. Ta is not commonly found in Ni-based wrought superalloys but is frequently used in Ni-based single crystal superalloys. This discrepancy arises because excessive γ′-phase-forming elements can increase the deformation resistance in Ni-based wrought superalloys, thereby diminishing their cold or hot workability[68]. Conversely, Ni-based single crystal superalloys are cast directly without undergoing cold or hot working processes, allowing for the inclusion of higher amounts of γ′-phase-forming elements.

The Ta content can varies from 3 wt% to 12 wt% and the total amount of main γ′- phase-forming elements(Al+Ti+Ta) could exceed up to 20 wt%[69,70]. As a result, the volume fraction of γ′ phase of Ni-based single crystal superalloys can surpass 60 wt%[71–74]. Researchers have shown that Ta inhibits the coalescence of the γ′ phase during isothermal long-term aging, thereby improving the microstructure stability of the γ′ phase and increasing its volume fraction[74–78]. Additionally, Ta can enhance oxidation and thermal corrosion resistance of superalloys in certain conditions[79,80].

The addition of Al, Ti, Nb and Ta of GH4350 actively contributes to maintaining the structural integrity and stability of the γ′ phase, effectively inhibiting its dissolution or structural alterations at elevated temperatures. Consequently, the γ′ phase continues to impede dislocation motion at high temperatures, thereby strengthening the alloy. This enhancement in γ′ phase stability is pivotal for ensuring the alloy retains its desired properties.
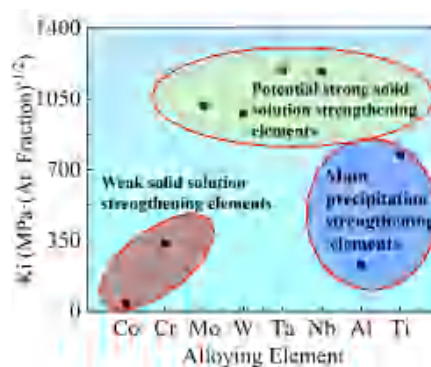

Fig. 2 Strengthening constants for solid solution strengthening in Ni. (adapted from Ref. [51])

1.2 The precipitation phases of GH4350

Many studies have demonstrated that the precipitation phases of GH4350 are γ′ phase and η phase [12–15,20–22,28,56,68,81,82]. The crystal structure of η phase is shown in Fig. 3(a). Apparently, the stacking sequence is ABACABAC……which is a typical kind of HCP crystal structure. Fig. 3(b) and (c) indicates the microstructure of γ′ phase and η phase by transmission electron microscope

(TEM) and the chemical compositions of them of alloy K4750 respectively. The energy dispersive spectrometer (EDS) results show that the η phase are primarily composed of Ni, Al, Ti, Nb, which are close to the chemical composition of γ′ phase.

1.3 Heat treatment of GH4350

1.3.1 Homogenization of as-cast GH4350

Due to their high degree of alloying, wrought superalloys often experience severe dendritic segregation during solidification, leading to poor hot workability[83]. To eliminate the segregation, an appropriate homogenization heat treatment process is essential and is the first step to obtain the target microstructure[83–85]. In the as-cast state of GH4350 prepared by VIM+VAR, significant elemental segregation occurs with Nb, Ti and Ta elements enriched in the inter-dendrites, and Cr, Mo and Al elements enriched in the dendrites[11]. This segregation is accompanied by the precipitation of Laves phases and acicular phases in the inter-dendrites, while

dispersed γ′ phases are also precipitated during the cooling process[11]. To mitigate these issues, a homogenization heat treatment at 1180 °C for 40 h with furnace cooling has been proposed, successfully eliminating elemental segregation and detrimental phases[11]. Achieving a uniform microstructure with consistent elemental composition requires a relatively long heat treatment time, and researches on homogenization heat treatments are limited. Therefore, careful design of the melting and homogenization processes is crucial.

1.3.2 Solid solution heat treatment of GH4350

Precipitation phases can be detrimental if they form excessively during solidification, as they can act as sources of cracks. However, these phases are also crucial for precipitation strengthening. Therefore, a comprehensive understanding of the control of precipitation phases in GH4350 is essential. Scanning electron microscope (SEM) observations of samples solution-treated at various temperatures for 1h
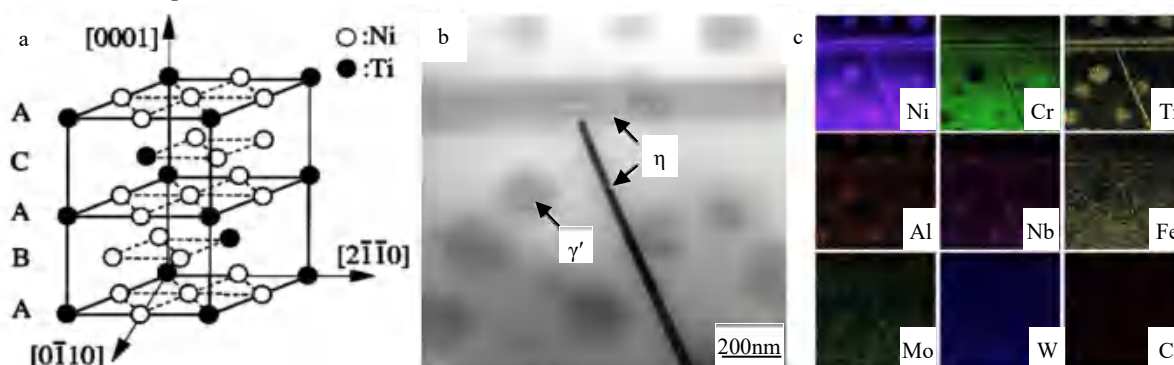

Fig. 3 Crystal structure and chemical composition of η phase. (a) Crystal structure of η phase. (b) The TEM image of γ′ and η phase and (c) the corresponding EDS mapping of alloy K4750. (adapted from Refs. [86,87])

are shown in Fig. 4. The γ′ phases begin to dissolve at 1010 °C which aligns well with the solvus temperature of γ′ phases reported in other literatures[12,81].

As indicated in Fig. 4, the η phase is significantly reduced

at 1055 °C. When the temperature rises to 1080 °C, only sporadic η phase can be observed and it is completely dissolved at 1095 °C.
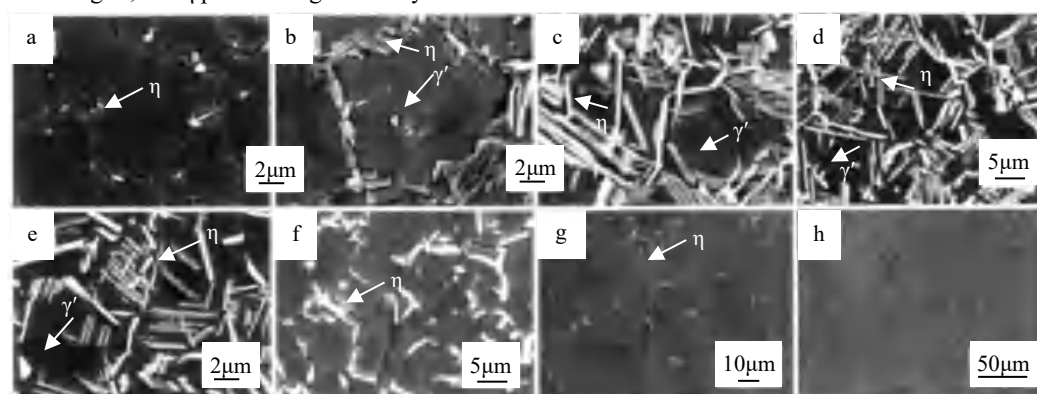

Fig. 4 SEM observations of samples solution-treated at different temperatures for 1 h. (a)~(h) are solution-treated at 830 °C, 950 °C, 980 °C, 1010 °C, 1020 °C, 1055 °C, 1080 °C and 1095°C respectively. (adapted from Ref. [82])

If the alloy is solid-solution treated below the solvus temperature of the η phase, such as at 1050 °C, the precipitation of

the η phase at grain boundaries may be utilized to control grain size like δ phase[20,88]. As the temperature increases from 800 °C

to 1070 °C, the recrystallized grain size increases slightly from approximately 10 μm to 14 μm while further increasing temperature from 1080 °C to 1095 °C, the grain size increases significantly, approaching 100 μm, due to the lack of η phase pinning at the grain boundaries[82]. Most reported solid-solution temperatures of GH4350 are above the solvus temperature of the η phase[12,13,15,21,68,89]. It appears that controlling grain size with the η phase is not the primary focus of the solid-solution treatment but the complete dissolution of η phase into the matrix is the ultimate goal. This approach may help to prevent the continued growth of the η phase during solid solution heat treatment[22].

1.3.3 Aging treatment of GH4350

Aging treatments are performed after solid solution to optimize the precipitations of γ′ and η phases[90]. The lower limit temperature of γ′ phase precipitation is determined to be between
650 °C and 700 °C based on variation in hardness over aging time and temperature (Fig. 5(a)) for solution-treated GH4350 alloy[12,81].

During aging treated at 788 °C, the η phase is observed at the grain boundaries (Fig. 5 (b), point C_1), indicating that the lower limit for η phase precipitation is approximately 788 °C. When the aging temperature is further increased to 816 °C, maximum hardness is achieved at both solid solution temperatures. As seen at point D_1 in Fig. 5(b), both γ′ and η phases are present.

As indicated in Fig. 5(c) through (f), the growth and morphology of the η phase vary with different heat treatments. Initially, the plate-like η phase precipitates at the grain boundaries (Fig. 5(c) and (d)). With increasing aging temperature and time,

the η phase progressively grows from the grain boundaries to the grains, forming a Widmanstätten morphology structure (Fig. 5(e) and (f)).

In conclusion, the precipitation and distribution characteristics of the η phase are significantly affected by the aging heat treatment. A comprehensive understanding of the effect of heat treatment on γ′ and η phases precipitation is required to develop a rational heat treatment strategy.

1.4 Phase transformation behaviors

From the perspective of phase stability, the η phase is a more stable at temperatures of 650 °C or above, which is confirmed by thermodynamic calculations of the phase stability of Nimonic 263 that show the γ′ phase is stable up to 750 °C while η phase is stable up to 957 °C[91]. Long-term thermal exposure further supports this, as the η phase predominates throughout the matrix, and nearly all γ′ particles dissolve when the alloy is exposed to 870 °C for 8000 h[92].

The chemical compositions of the γ′ and η phases are similar with their primary distinction being their crystal structures. The γ′ to η transformation occurs through the introduction of stacking faults into the γ′ phase formed by the systematic passage of Shockley partials[68,87,91–96]. As shown in Fig. 6, theoretically, if one A layer is added by the introduction of extrinsic stacking faults in γ′ between B layer and C layer, the stacking sequence will become ABACABAC ... which is actually identical to the stacking sequence along the close packed planes (0001) in η phase. Experimental observations, as shown in Fig. 7(a)~(d), indicate that the η phase grows at the expense of γ′ phase, with γ′ precipitation-free zones (PFZs) forming around each η precipitate. The above information suggests a close relationship between η phase formation, the γ′ phase, and stacking
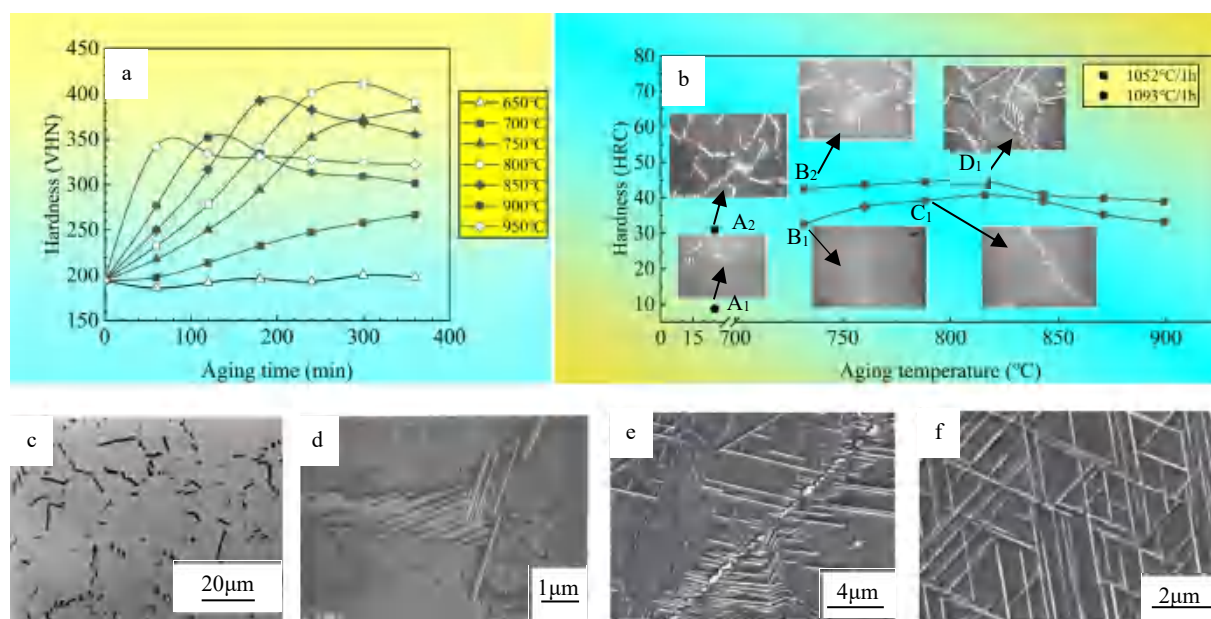

Fig. 5 Microstructures corresponding to different heat treatment and their associated hardness values. (a) Variation of hardness with aging time for solution-treated GH4350 at various temperatures. (b) Variation of hardness with aging temperature for solution-treated GH4350 and the

corresponding microstructures for several typical points (A to D). (c) and (d) are both solid solution-treated at approximately 1050 ℃ for 1h but aging-treated at 750 ℃ for 1h and at 899 ℃ for 4h+816 ℃ for 4h respectively. (e) and (f) are solid solution treated at 1100 ℃ for 1h+ aging-treated at 1000 ℃ for 3h and (e) is grain boundary area while (f) is grain interior. (adapted from Refs. [12,22,81])
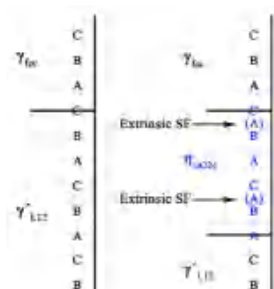

Fig. 6 Illustration of the γ′ to η transformation by the introduction of extrinsic stacking faults. (adapted from Refs. [86,87])

faults. Additionally, Fig. 7(e)~(h) demonstrates that stacking faults, induced by numerous paired dislocations, appear to elongate and eventually transform into the growing η phase at the expense of γ′ phase.

More precise evidence in experiment indicates that two-layer extrinsic faults found in γ′ phase (Fig. 8(a) and (b)) are formed by the passage of two identical 1/6<112> shockley partials on consecutive {1 1 1} planes and η phase forming elements (i.e., Ta, Nb, Ti) are segregated along superlattice extrinsic stacking faults(SESFs) confirmed by high spatial resolution energy dispersive X-ray spectroscopy(EDX) mapping (Fig. 8(c))[93,94].

These observations indicate that stacking faults in the γ′ phase may serve as local nucleation sites for the η phase. Fig. 9(a) and (b) shows that the nucleation and growth of η phase have two paths which η phase directly precipitates within extra-large γ′ (EL-γ′) when the coalescence of γ′ phases reaches a critical stage or η phase precipitates at the interface between small

MC carbides and EL-γ′ with both MC carbides and η embedded within EL-γ′[40].

Interestingly, as shown in Fig. 9(c) and (d), both paths share a common feature: they both lead to the formation of stacking faults. Notably, MC carbides are segregated with Ti and the nucleation and growth of η phase in the second path (with MC-II carbide) occur more rapidly than in the first path (without carbide)[40]. This suggests that MC-II carbide is a more effective provider of η phase-forming elements compared to EL-γ′ in this study.

Based on the preceding discussion, two criteria for the formation and growth of the η phase can be concluded: (1) stacking faults initially serve as nucleation sites, and (2) sufficient η phase-forming elements must be present during nucleation and growth. To better regulate the microstructure and, consequently, the properties of superalloys, further research into the mechanisms of η phase nucleation and growth is necessary. This will enhance our understanding and control over η phase development.

2 Roles of η phase

To address the need for higher operating temperatures in fasteners, increasing the amount of γ′ phase strengthening elements may enhance high-temperature performance. However, at temperatures above 650 ℃, the γ′ to η phase transformation occurs, leading to a decrease in the γ′ phase volume fraction and consequently reducing its reinforcing effect. Therefore, understanding the impact of the η phase on the properties of superalloys is crucial.
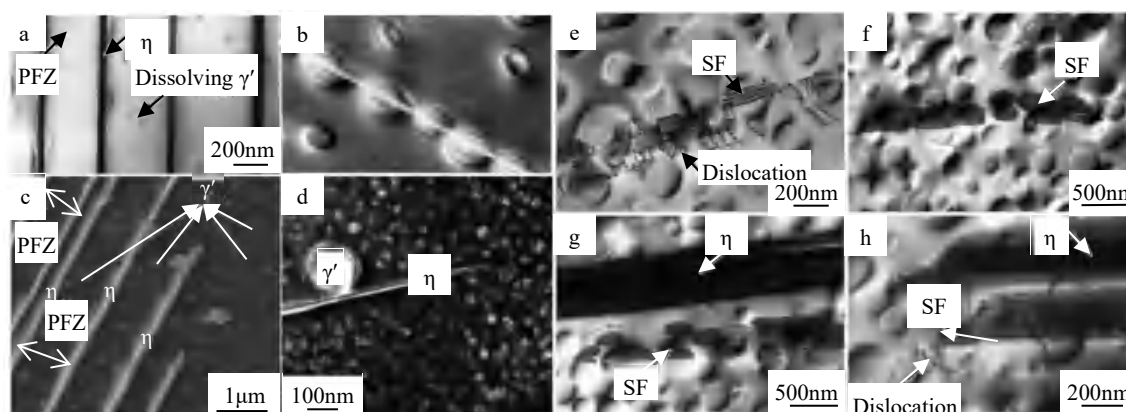

Fig. 7 Typical micrographs of η phase growing by consuming γ′ phase of various superalloys. (a) Alloy K4750. (b) Alloy GH4350. (c) Alloy A286. (d) Alloy 718 plus. (e)~(h) are TEM images of stacking faults and η phase in K4750. (adapted from Refs. [68,87,95,96])
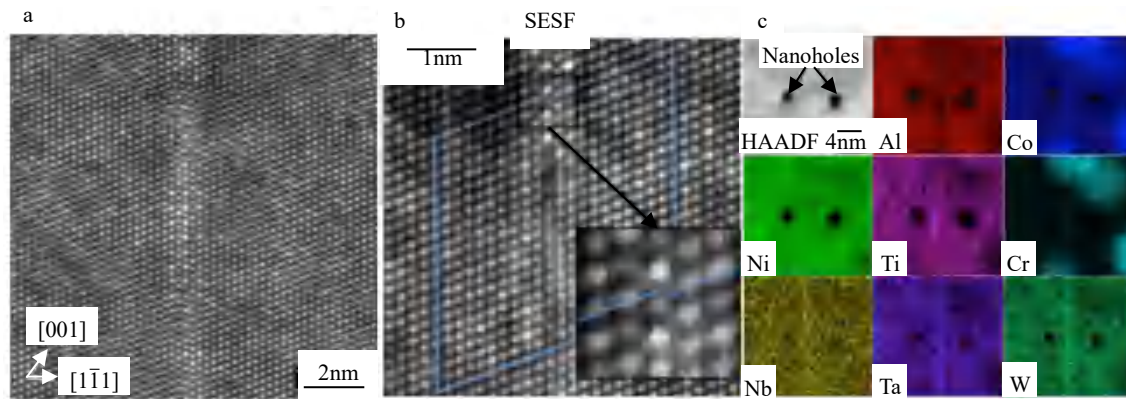
Fig. 8 More precise evidence of γ′ phase to η phase transformation in experiment. (a) High angle angular dark field-scanning transmission electron microscope (HAADF-STEM) images of a grid-like ordering along a SESF inside a γ′ precipitate; (b) Shockley partials at leading SESF showing by burgers circuit analysis. (c) EDX elemental map of a vertical SESF showing segregation along the fault. (adapted from Ref. [93])
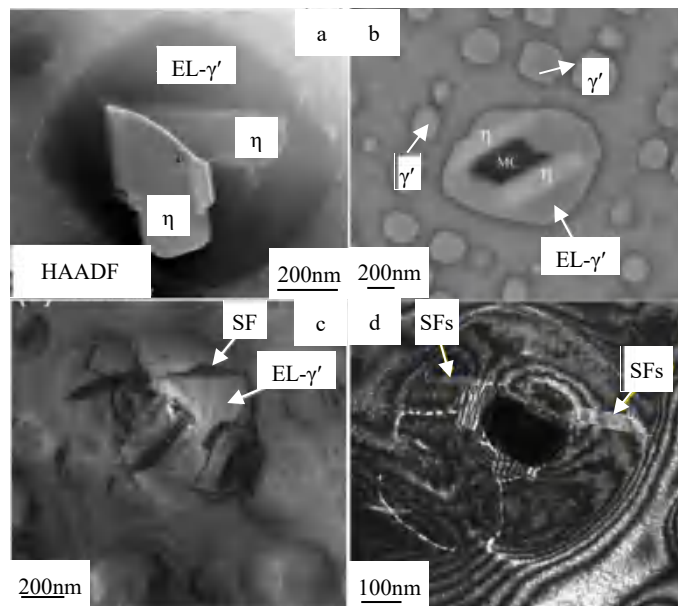

Fig. 9 Two paths of η phase formation. (a) Precipitate directly within EL-γ′. (b) Precipitate at the interface of small size MC carbides and EL-γ′. (c) and (d) are the formation of stacking faults in both paths, respectively. (adapted from Ref. [40])

As previously discussed, the η phase initially precipitates at the grain boundaries (intergranular) and evolves into a Widmanstätten morphology with increased time and temperature (intragranular). Researchers have identified four distinct forms of the η phase—needle-like, plate-like, granular, and short rod-like (Fig. 10), each of which impacts the properties of superalloys differently[23,95].
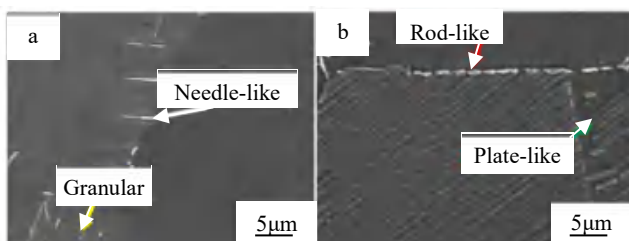
Fig. 10 Needle-like, plate-like, granular and short rod-like η phase. (adapted from Ref. [23])

This characteristic affects the morphology of grain boundaries, significantly impacting superalloy strengthening. It is reported that the discontinuous precipitation of plate-like η phase exerts a pinning effect on the grain boundary, leading to the formation of grain boundary serrations whose magnitude is increased with the increase of the inclination angle with respect to the grain boundaries[6,29,95]. Grain boundary serrations, intergranular and intragranular η phase influence the properties of superalloys.

2.1 The effects of η phase on crack initiation and propagation

Serrated grain boundaries induced by η phase can enhance the creep resistance by reducing cavitation and crack propagation rates and they also appear to retard the propagation of intergranular cracks to some extent during

fatigue test[25,26]. This suggests a potential beneficial effect of the η phase-induced serrated grain boundaries in impeding crack propagation along grain boundaries.

Additionally, small η phases at grain boundaries typically do not initiate cavities during creep though dislocations piled up ahead of them[87]. As shown in Fig. 11(a), 2 to 3% area fraction of η phase which extended from grain boundaries across the PFZs may be beneficial to creep strength and ductility by constraining grain boundary cavity growth[24]. These findings collectively indicate that the η phases whether in small sizes at grain boundaries or within a limited area fraction may not necessarily have a detrimental effect on creep properties. Instead, in certain configurations, they may exhibit a neutral or even a beneficial role in enhancing creep strength and ductility by impeding cavity growth along grain boundaries.

However, as illustrated in Fig. 11(b) and (c), cracks tend to form around the η phases, indicating intergranular η phase may act as brittle sites at the grain boundaries, thus serving as sites for crack initiation during creep tests[27]. During the fatigue processes, stress concentration as a result of dislocations accumulation and networks formation at the edges of η precipitates can induce the initiation and propagation of micro-cracks[25]. These observations suggest that the impact of η phases on crack initiation and propagation varies depending on specific conditions, such as loading type (creep or fatigue) and microstructural characteristics, underscoring the complexity and multifaceted nature of the η phase in superalloys.

Understanding the circumstances under which the η phase acts as a crack initiation site or stress concentrator versus when it potentially impedes crack propagation is crucial. This understanding will greatly aid in optimizing superalloy designs to harness beneficial effects or mitigate detrimental influences of the η phase on properties.
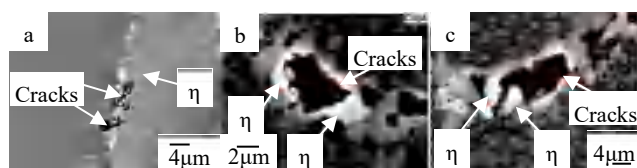

Fig. 11 The role of η phase during creep test. (a) Two grain boundary cavities whose growth appears to be constrained by impingement on η phase platelet. (b) and (c) are backscattered electron micrographs of STAL15-CC alloy after creep at 850 ℃ showing secondary cracks forming around η layers at grain boundaries. (adapted from Refs. [24,27])

2.2 The effects of η phase on dislocation hindering

As a precipitation phase, η phase is expected to contribute to precipitation strengthening similar to the γ′ phase. For instance, with aging time extending from 25 h to 100 h, the ultimate tensile strength (UTS) of alloy ATI 718Plus significantly improves from 797 MPa to 860 MPa with an increased volume fraction of plate-like/needle-like η phases[23]. Notably, during this period, the volume fraction of γ′ phase decreases from approximately 32 % to 28 %[23]. This suggests that the strengthening effect of the γ′ phase is comparatively weaker. Consequently, the observed enhancement in tensile properties is attributed to the precipitation of a significant amount of plate-like and needle-like η phases. TEM observations further confirm that the improved UTS is due to the hindrance of dislocation motion at grain boundaries and within grains near the η phases (Fig. 12(a) and (c)).

The effect of η phase on dislocation hindering is also reported in a research of stress relaxation behavior of GH4350, it is concluded that the enhanced stress relaxation resistance at 800 ℃ is attributed to the dislocation blocking by η phases, as shown in Fig. 12(d)[15]. This study also compares the stress relaxation resistance of Waspaloy and GH4350 at various temperatures. At 600 ℃, dislocations are still impeded by intragranular η phases (Fig. 12(b)), however, the larger size and higher mass fraction of γ′ phases in Waspaloy are key factors in hindering the movement of dislocations while the amount of intragranular η phases in GH4350 is rather small, thus η phases contribute little to the relaxation resistance at this temperature, leading a better stress relaxation resistance of Waspaloy than that of GH4350[15].
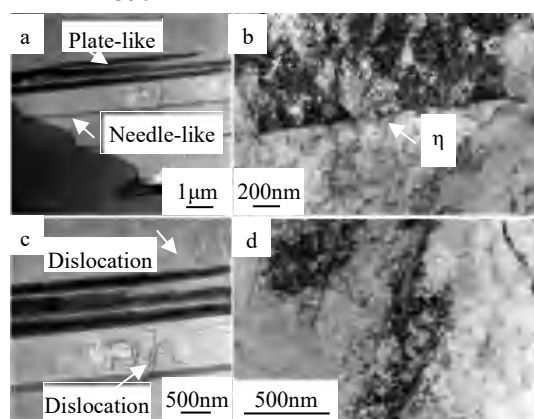

Fig. 12 Bright-field TEM observations of η phases and the dislocations. (a) Grain boundary η phases and the dislocations in the grain, (c) is the high magnifications of (a). (b) and (d) are microstructures of GH4350 after relaxation at 600 ℃ and 800 ℃ respectively. (adapted from Refs.[15,23])

3 Conclusions

1) GH4350 incorporates significant amounts of Co, Mo, and W to enhance solid solution strengthening, as quantified through modeling, and maintains a moderate (Al+Ti+Nb) content to balance precipitation strengthening with deformability. The addition of Ta not only stabilizes and increases the volume fraction of the γ′ phase but also improves oxidation and thermal corrosion resistance.

2) The primary precipitation phases in GH4350 are γ′ and η, which can be controlled through heat treatment at various temperatures and durations. A homogenization heat treatment at

1180 °C for 40 h with furnace cooling effectively removes elemental segregation and undesirable phases, providing a foundation for subsequent phase control.

3) The lower temperature limit for γ′ phase precipitation is between 650 °C and 700 °C, with a solvus temperature around 1010 °C. For η phase, precipitation begins at approximately 788 °C. As temperature and time increase, η phase precipitates from grain boundaries into the grains, developing a Widmanstätten morphology, and eventually dissolves completely at temperatures nearing 1080 °C. Solid solution heat treatment below this temperature may be able to control grain size through the undissolved η phase.

4) The γ′ to η phase transformation occurs because η phase is more stable above 650 °C. Both phases share similar elemental compositions and transformable crystal structures, facilitated by the introduction of stacking faults. This transformation is accelerated in the presence of effective η phase-forming elements providers, such as MC-type carbides, surrounding the γ′ phase.

5) Small quantities of η phase with needle-like, plate-like, granular, and short rod-like morphologies can improve properties such as creep resistance, tensile strength, fatigue resistance, and stress relaxation resistance by reducing cavitation, crack propagation, and hindering dislocation movement. Conversely, a large volume of η phase with Widmanstätten morphology can negatively impact mechanical properties, as the brittleness of η phase and associated stress concentrations lead to crack initiation and growth, ultimately depleting γ′ phase and diminishing its strengthening effect.

References

1   PAN Y, WEN M. Ab-initio calculations of mechanical and thermodynamic properties of TM (transition metal: 3d and 4d)-doped Pt3Al[J]. *Vacuum*, 2018, 156: 419-426.

2   PAN Y, PU D L, LI Y Q, et al. Origin of the antioxidation mechanism of RuAl(1 1 0) surface from first-principles calculations[J]. *Materials Science and Engineering: B*, 2020, 259: 114580.

3   PAN Y, YANG F. Influence of pressure on the structural, elastic and thermodynamic properties of α- and β- PtAl high temperature alloys[J]. *Journal of Materials Research and Technology*, 2024, 28: 381-389.

4   PAN Y. Vacancy-induced mechanical and thermodynamic properties of B2-RuAl[J]. *Vacuum*, 2017, 143: 165-168.

5   LIANG L, XU M, CHEN Y, et al. Effect of welding thermal treatment on the microstructure and mechanical properties of nickel-based superalloy fabricated by selective laser melting[J]. *Materials Science and Engineering: A*, 2021, 819: 141507.

6   PICKERING E J, MATHUR H, BHOWMIK A, et al. Grain-boundary precipitation in Allvac 718Plus[J]. *Acta Materialia*, 2012,

60(6-7): 2757-2769.

7   CHEN T W, WANG P T, KANG Y C, et al. Grain boundary serration tuning and its effect on hot workability of a wrought superalloy[J]. *Journal of Alloys and Compounds*, 2023, 960: 170620.

8   FECHT H, FURRER D. Processing of Nickel-Base Superalloys for Turbine Engine Disc Applications[J]. *Advanced Engineering Materials*, 2000, 2(12): 777-787.

9   PAN Y. Exploring the phase stability, mechanical and thermodynamic properties of FeCrAl ternary alloy[J]. *Journal of Materials Research and Technology*, 2023, 26: 8813-8821.

10   MELHEM G N. Encyclopedia of Aluminum and Its Alloys, Two-Volume Set (Print) [M]. 1st ed. Boca Raton: CRC Press, 2018.

11   LI K, YANG Y, WANG Z, et al. Micro-segregation and homogenizing treatment of GH350 ingot[J].   *Journal of Iron and Steel Research International*, 2012, 24(7): 54-58. (in Chinese)

12   ASGARI S. Age-hardening behavior and phase identification in solution-treated AEREX 350 superalloy[J]. *Metallurgical and Materials Transactions A,* 2006, 37(7): 2051-2057.

13   NAJAFI H, ASGARI S. Strain hardening mechanisms in aged AEREX350 superalloy[J]. *Materials Science and Engineering: A*, 2005, 398(1-2): 204-208.

14   JIANG H, YANG J, DONG J, et al. Stress Relaxation Behavior Comparison of Typical Nickel-Base Superalloys for Fasteners[C]// Proceedings of the 9th International Symposium on Superalloy 718 & Derivatives: Energy, Aerospace, and Industrial Applications. Cham: Springer International Publishing, 2018: 789-804.

15   WANG Y, DONG J, ZHANG M, et al. Stress relaxation behavior and mechanism of AEREX350 and Waspaloy superalloys[J]. *Materials Science and Engineering: A*, 2016, 678: 10-22.

16   JIANG H, DONG J, ZHANG M, et al. Stress Relaxation Mechanism for Typical Nickel-Based Superalloys Under Service Condition[J]. *Acta Metall Sin*, 2019, 55(9): 1211-1220. (in Chinese)

17   FERRERO J G. Candidate materials for high-strength fastener applications in both the aerospace and automotive industries[J]. *Journal of Materials Engineering and Performance*, 2005, 14(6): 691-696.

18   SPS TECHNOLOGY. Superalloys Developed by SPS Technologies for Aerospace Fasteners [EB/OL].

19   DU J, LV X, DONG J, et al. Research progress of wrought superalloys in China[J]. *Acta Metall Sin*, 2019, 55(9): 1115-1132. (in Chinese)

20   SAMIEE M, ASGARI S. Influence of solution treatment on precipitation behavior of a Ni–Co alloy[J]. *Scripta Materialia*, 2007, 57(2): 93-96.

21   FARVIZI M, ASGARI S. Effects of cold work prior to aging on

microstructure of AEREX™350 superalloy[J]. *Materials Science and Engineering: A*, 2008, 480(1): 434-438.

22   KERMAJANI M. Influence of double aging on microstructure and yield strength of AEREX™ 350[J]. *Materials Science and Engineering: A*, 2012, 534: 547-551.

23   LI J, WU Y, LIU Y, et al. Enhancing tensile properties of wrought Ni-based superalloy ATI 718Plus at elevated temperature via morphology control of η phase[J]. *Materials Characterization*, 2020, 169: 110547.

24   SHINGLEDECKER J P, PHARR G M. The Role of Eta Phase Formation on the Creep Strength and Ductility of INCONEL Alloy 740 at 1023 K (750 °C)[J]. *Metallurgical and Materials Transactions A*, 2012, 43(6): 1902-1910.

25   QI Q, ZHANG H, LIU C, et al. On the microstructure evolution during low cycle fatigue deformation of wrought ATI 718Plus alloy[J]. *Materials Science and Engineering: A*, 2020, 798: 140132.

26   HONG H U, KIM I S, CHOI B G, et al. The effect of grain boundary serration on creep resistance in a wrought nickel-based superalloy[J]. *Materials Science and Engineering: A*, 2009, 517(1): 125-131.

27   KONTIS P. Influence of composition and precipitation evolution on damage at grain boundaries in a crept polycrystalline Ni-based superalloy[J]. *Acta Materialia*, 2019.

28   ASGARI S. Structure and strain hardening of superalloy AEREX350[J]. *Journal of Materials Processing Technology*, 2001, 118(1-3): 246-250.

29   ALABBAD B, TIN S. Effect of grain boundary misorientation on η phase precipitation in Ni-base superalloy 718Plus[J]. *Materials Characterization*, 2019, 151: 53-63.

30   ZHAO Y, PENG J, ZHANG X, et al. Effect on solution holding time on microstructure and mechanical properties of GH4698 superalloy[J] *Heat Treatment of Metals*, 2016, 41(8): 56-59. (in Chinese)

31   DEVAUX A, NAZÉ L, MOLINS R, et al. Gamma double prime precipitation kinetic in Alloy 718[J]. *Materials Science and Engineering: A*, 2008, 486(1-2): 117-122.

32   HOSSEINI E, POPOVICH V A. A review of mechanical properties of additively manufactured Inconel 718[J]. *Additive Manufacturing*, 2019, 30: 100877.

33   SLAMA C, ABDELLAOUI M. Structural characterization of the aged Inconel 718[J]. *Journal of Alloys and Compounds*, 2000, 306(1-2): 277-284.

34   ZHANG M, MA C C, CHUN X, et al. Effect of Precipitate Phases and Grain Size on Mechanical Properties of Inconel 718 Superalloy After Various Heat Treatments[J]. *Rare Metal Materials and Engineering*, 2024, 53(8): 2131-2136.

35   KENNEDY R L. Allvac 718Plus, Superalloy for the Next Forty Years[C]// Superalloys 718, 625, 706 and Various Derivatives (2005). TMS, 2005: 1-14.

36   HASSAN B, CORNEY J. Grain boundary precipitation in Inconel 718 and ATI 718Plus[J]. *Materials Science and Technology*, 2017, 33(16): 1879-1889.

37   KIENL C, MANDAL P, LALVANI H, et al. Role of the Secondary Phase η During High-Temperature Compression of ATI 718Plus®[J]. *Metallurgical and Materials Transactions A*, 2020, 51(8): 4008-4021.

38   GÖKEN M, KEMPF M. Microstructural properties of superalloys investigated by nanoindentations in an atomic force microscope[J]. *Acta Materialia*, 1999, 47(3): 1043-1052.

39   KINZEL S, GABEL J, VÖLKL R, et al. Reasons for Volume Contraction after Long-Term Annealing of Waspaloy[J]. *Advanced Engineering Materials*, 2015, 17(8): 1106-1112.

40   LIU G, XIAO X, VÉRON M, et al. The nucleation and growth of η phase in nickel-based superalloy during long-term thermal exposure[J]. *Acta Materialia*, 2020, 185: 493-506.

41   AGNOLI A, LE GALL C, THEBAULT J, et al. Mechanical Properties Evolution of γ′/γ″ Nickel-Base Superalloys During Long-Term Thermal Over-Aging[J]. *Metallurgical and Materials Transactions A*, 2018, 49(9): 4290-4300.

42   WANG M X, ZHU H, YANG G J, et al. Solid-solution strengthening effects in binary Ni-based alloys evaluated by high-throughput calculations[J]. *Materials & Design*, 2021, 198: 109359.

43   KOU H, LI W, MA J, et al. Theoretical prediction of the temperature-dependent yield strength of solid solution strengthening Nickel-based alloys[J]. *International Journal of Mechanical Sciences*, 2018, 140: 83-92.

44   BUTT M Z. Solid-solution hardening in dilute and concentrated alloys[J]. *Philosophical Magazine Letters*, 1989, 60(4): 141-145.

45   GYPEN L A, DERUYTTERE A. The combination of atomic size and elastic modulus misfit interactions in solid solution hardening[J]. *Scripta Metallurgica*, 1981, 15(8): 815-820.

46   KRATOCHVÍL P, LUKÁČ P, SPRUŠIL B. On solid solution hardening in crystals with randomly distributed solute atoms[J]. *Czechoslovak Journal of Physics*, 1973, 23(6): 621-626.

47   LABUSCH R. A Statistical Theory of Solid Solution Hardening[J]. *physica status solidi (b)*, 1970, 41(2): 659-669.

48   FLEISGHER R L. Solution hardening[J]. Acta metallurgica, 1961, 9(11): 996-1000.

49   FLEISCHER R L. Substitutional solution hardening[J]. *Acta metallurgica*, 1963, 11(3): 203-209.

50   MISHIMA Y, OCHIAI S, HAMAO N, et al. Solid Solution

Hardening of Ni₃Al with Ternary Additions[J]. *Transactions of the Japan Institute of Metals*, 1986, 27(9): 648-655.

51　ROTH H A, DAVIS C L, THOMSON R C. Modeling solid solution strengthening in nickel alloys[J]. *Metallurgical and Materials Transactions A*, 1997, 28(6): 1329-1335.

52　MISHIMA Y, OCHIAI S, HAMAO N, et al. Solid solution hardening of nickel—role of transition metal and B-subgroup solutes—[J]. *Transactions of the Japan institute of metals*, 1986, 27(9): 656-664.

53　GYPEN L A, DERUYTTERE A. Multi-component solid solution hardening[J]. *Journal of Materials Science*, 1977, 12(5): 1034-1038.

54　CHEN Y T, YEH A C, LI M Y, et al. Effects of processing routes on room temperature tensile strength and elongation for Inconel 718[J]. *Materials & Design*, 2017, 119: 235-243.

55　CHEN X M, NING M T, HU H W, et al. Characterization of hot deformation behavior and optimization of hot workability for GH4698 superalloy[J]. *Materials Characterization*, 2023, 201: 112916.

56　HOSSEINIFAR M, ASGARI S. Static recrystallization behavior of AEREX350 superalloy[J]. *Materials Science and Engineering: A*, 2010, 527(27): 7313-7317.

57　LI K, HAN G, DENG B. Influence of aging treatment on microstructure and properties od cold-drawn alloy GH350[J]. *Acta Aeronautica et Astronautica Sinica*, 2012, 33(06): 1156-1162. (in Chinese)

58　YANG C L, ZHANG Z J, ZHANG P, et al. Synchronous improvement of the strength and plasticity of Ni-Co based superalloys[J]. *Materials Science and Engineering: A*, 2018, 736: 100-104.

59　GIESE S, BEZOLD A, PRÖBSTLE M, et al. The Importance of Diffusivity and Partitioning Behavior of Solid Solution Strengthening Elements for the High Temperature Creep Strength of Ni-Base Superalloys[J]. *Metallurgical and Materials Transactions A*, 2020, 51(12): 6195-6206.

60　FAYMAN Y. C. γ-γ′ Partitioning Behaviour in Waspaloy[J]. *Materials Science and Engineering*, 1986, 82, 203-215.

61　KARUNARATNE M S A, REED R C. Interdiffusion of Niobium and Molybdenum in Nickel between 900 -1300 °C[J]. *Defect and Diffusion Forum*, 2005, 237-240: 420-425.

62　JUNG S B, YAMANE T, MINAMINO Y, et al. Interdiffusion and its size effect in nickel solid solutions of Ni-Co, Ni-Cr and Ni-Ti systems[J]. *Journal of Materials Science Letters*, 1992, 11(20): 1333-1337.

63　HE C, LIU L, HUANG T, et al. Effect of aging temperature on the secondary γ′ precipitation in a model Ni based single crystal superalloy[J]. *Journal of Alloys and Compounds*, 2020, 836: 155486.

64　PRÖBSTLE M, NEUMEIER S, FELDNER P, et al. Improved creep strength of nickel-base superalloys by optimized γ/γ′ partitioning behavior of solid solution strengthening elements[J]. *Materials Science and Engineering: A*, 2016, 676: 411-420.

65　KARUNARATNE M S A, CARTER P, REED R C. Interdiffusion in the face-centred cubic phase of the Ni–Re, Ni–Ta and Ni–W systems between 900 and 1300°C[J]. *Materials Science and Engineering: A*, 2000, 281(1-2): 229-233.

66　KARUNARATNE M S A, CARTER P, REED R C. On the diffusion of aluminium and titanium in the Ni-rich Ni–Al–Ti system between 900 and 1200°C[J]. *Acta Materialia*, 2001, 49(5): 861-875.

67　CHENG Y, ZHAO X, YUE Q, et al. Research Progress of Effects of Mo and W on Ni-based Single Crystal Superalloys[J]. *Rare Metal Materials and Engineering*, 2023, 52(7): 2599-2611.(in Cninese)

68　ASGARI S, SHARGHI-MOSHTAGHIN R, SADEGHAHMADI M, et al. On phase transformations in a Ni-based superalloy[J]. *Philosophical Magazine*, 2013, 93(10-12): 1351-1370.

69　XIA W, ZHAO X, YUE L, et al. A review of composition evolution in Ni-based single crystal superalloys[J]. *Journal of Materials Science & Technology*, 2020, 44: 76-95.

70　LONG H, MAO S, LIU Y, et al. Microstructural and compositional design of Ni-based single crystalline superalloys ― A review[J]. *Journal of Alloys and Compounds*, 2018, 743: 203-220.

71　ALI M A, LÓPEZ-GALILEA I, GAO S, et al. Effect of γ′ precipitate size on hardness and creep properties of Ni-base single crystal superalloys: Experiment and simulation[J]. *Materialia*, 2020, 12: 100692.

72　YANG W, YUE Q, CAO K, et al. Negative influence of rafted γ′ phases on 750 °C/750 MPa creep in a Ni-based single crystal superalloy with 4% Re addition[J]. *Materials Characterization*, 2018, 137: 127-132.

73　SHUI L, JIN T, TIAN S, et al. Influence of precipitate morphology on tensile creep of a single crystal nickel-base superalloy[J]. *Materials Science and Engineering: A*, 2007, 454-455: 461-466.

74　WU J, JIANG X, WANG Y, et al. Effects of Ta on microstructural stability and mechanical properties of hot corrosion resistant Ni-based single crystal superalloys during long-term thermal exposure[J]. *Materials Science and Engineering: A*, 2021, 806: 140829.

75　COSTA A M S, OLIVEIRA J P, SALGADO M V, et al. Effect of Ta and Nb additions in arc-melted Co-Ni-based superalloys: Microstructural and mechanical properties[J]. *Materials Science and Engineering: A*, 2018, 730: 66-72.

76　PENG P, LU L, LIU Z, et al. Investigation on the influence of Ta on the microstructure evolution of Ni-based superalloy DZ411 during directional solidification, heat treatment, and long-term aging[J]. *Journal of Alloys and Compounds*, 2022, 920: 165886.

77　XU Y, WANG T, LV X. Effect of Ta and Mo point preference on

the γ′ phase of Co-Al-W superalloy[J]. *Rare Metal Materials and Engineering*, 2023, 52(11): 3939-3946. (in Chinese)

78　LAI Y, NING L, ZHAO L, et al. Effects of Ta and Co on Microstructural Stability of a Novel High Strength and Hot Corrosion Resistant Single Crystal Superalloys[J]. *Rare Metal Materials and Engineering*, 2024, 53(3): 748-756. (in Chinese)

79　PARK S J, SEO S M, YOO Y S, et al. Effects of Al and Ta on the high temperature oxidation of Ni-based superalloys[J]. *Corrosion Science*, 2015, 90: 305-312.

80　HAN F F, CHANG J X, LI H, et al. Influence of Ta content on hot corrosion behaviour of a directionally solidified nickel base superalloy[J]. *Journal of Alloys and Compounds*, 2015, 619: 102-108.

81　TOMASELLO C M, PETTIT F S, BIRKS N, et al. Precipitation Behavior in AEREX(TM) 350[C]// *Superalloys*. TMS, 1996:145-51.

82　WAN W, HAN G, DENG B. Influence of solution treatment on microstructure of AEREX350 alloy[J]. *Journal of Iron and Steel Research International*, 2010, 17(3): 67-71.

83　DONG J, LI L, LI H, et al. Effect of extent of homogenization on the hot deformation recrystallization of superalloy ingot in cogging process[J]. *Acta Metall Sin*, 2015, 51(10): 1207-1218. (in Chinese)

84　LIANG X, ZHANG R, YANG Y, et al. An Investigation of the Homogenization and Deformation of Alloy 718 Ingots[C]//*Superalloys 718, 625, 706 and Various Derivatives (1994)*. TMS, 1994: 947-956.

85　ZHANG X, CHEN J, YANG W, et al. Identification of precipitates in the as-cast microstructure and its evolution behavior during homogenization of a difficult-to-deform GH4141 superalloy[J]. *Rare Metal Materials and Engineering*, 2024, 53(1): 136-147. (in Chinese)

86　HAGIHARA K, NAKANO T, UMAKOSHI Y. Plastic deformation behaviour in Ni3Ti single crystals with D024 structure[J]. *Acta Materialia*, 2003, 51(9): 2623-2637.

87　HOU K, OU M, WANG M, et al. Precipitation of η phase and its effects on stress rupture properties of K4750 alloy[J]. *Materials Science and Engineering: A*, 2019, 763: 138137.

88　YANG Z, CHEN Z, LIN Y, et al. Effect of the aging and recrystallization annealing treatment on the forged mixed grain structure of Ni-based superalloy[J]. *Rare Metal Materials and Engineering*, 2023, 52(9): 3147-3152. (in Chinese)

89　WAN W, HAN G, DENG B. Influence of aging treatment on precipitation behavior of η phase in Ni-Co-Cr alloy[J]. *Journal of Iron and Steel Research International*, 2010, 17(1): 64-69.

90　WANG G, SONG W, LIANG J, et al. Effect of heat treatment on microstructure and tensile properties of a new type of Ni-base superalloy designed for additive manufacturing[J]. *Rare Metal Materials and Engineering*, 2024, 53(3): 787-795. (in Chinese)

91　ZHAO J C, RAVIKUMAR V, BELTRAN A M. Phase precipitation and phase stability in Nimonic 263[J]. *Metallurgical and Materials Transactions A*, 2001, 32(6): 1271-1282.

92　KIM I S, CHOI B G, HONG H U, et al. Influence of thermal exposure on the microstructural evolution and mechanical properties of a wrought Ni-base superalloy[J]. *Materials Science and Engineering: A* 2014, 593: 55-63.

93　SMITH T M, ESSER B D, ANTOLIN N, et al. Segregation and η phase formation along stacking faults during creep at intermediate temperatures in a Ni-based superalloy[J]. *Acta Materialia*, 2015, 100: 19-31.

94　SMITH T M, ESSER B D, ANTOLIN N, et al. Phase transformation strengthening of high-temperature superalloys[J]. *Nature Communications*, 2016, 7(1): 13434.

95　TANG L, ZHANG H, GUO Q, et al. The precipitation of η phase during the solution treatments of Allvac 718Plus[J]. *Materials Characterization*, 2021, 176: 111142.

96　SEIFOLLAHI M, RAZAVI S H, KHEIRANDISH Sh, et al. The Mechanism of η Phase Precipitation in A286 Superalloy During Heat Treatment[J]. *Journal of Materials Engineering and Performance*, 2013, 22(10): 3063-3069.

镍基变形高温合金 GH4350 的微观结构特征和强化特点综述

金巨烽 [1,2]，赵新宝 [1,3]，赵倩敏 [1,2]，岳全召 [1]，谷月峰 [1,3]，张泽 [1,3]

(1. 浙江大学 高温合金研究所 材料科学与工程学院，浙江 杭州 3110027)

(2. 浙江大学 工程师学院，浙江 杭州 3110027)

(3. 浙江大学 硅及先进半导体材料全国重点实验室，浙江 杭州 3110027)

摘 要： GH4350(AEREX 350)是一种紧固件用镍基变形高温合金，最高使用温度可达 750℃；GH4350 具备高抗拉强度的同时，能抗疲劳、抗应力断裂、抗应力松弛和耐腐蚀，并具备低膨胀系数和缺口敏感性。该合金主要通过固溶强化以及 γ′相沉淀强化，在 γ′相析出的同时也会析出少量 η 相。研究人员指出，该合金的微观结构对热处理条件包括温度和时间十分敏感，γ′相在某些热处理条件下会转变为 η 相，从而可能降低合金的性能。本综述概述了 GH4350 的元素组成特点、受热处理调控的微观结构特征以及强化特点，旨在理解该合金性能优异的原因，并指导新型合金或性能优化型合金的开发，以进一步提高其承温能力。

关键词： 紧固件用变形高温合金GH4350; 高温性能; 元素组成; 热处理; η相

Journal of Alloys and Compounds 期刊接收邮件

网络收录地址：

Doi: https://doi.org/10.1016/j.jallcom.2025.180231

期刊论文封面

View PDF   Download full issue

Outline

Highlights
Abstract
Keywords
1. Introduction
2. Experimental procedures
3. Results
4. Discussion
5. Conclusion
CRediT authorship contribution statement
Declaration of Competing Interest
Acknowledgements
Data availability
References

Show full outline ∨

Figures (17)

Journal of Alloys and Compounds
Volume 1024, 20 April 2025, 180231

Morphology control of η phase in enhancing high-temperature tensile property of superalloy GH4350

Jufeng Jin [a][b], Xinbao Zhao [a][c] ☉ ✉, Qianmin Zhao [a][b], Jiachen Xu [a], Yunpeng Fan [a], Wei Liu [a], Quanzhao Yue [a], Wanshun Xia [a] ☉ ✉, Xiao Wei [a][c], Yuefeng Gu [a][c] ☉ ✉, Ze Zhang [a][c]

Show more ∨

+ Add to Mendeley   ⌁ Share   🔗 Cite

https://doi.org/10.1016/j.jallcom.2025.180231 ↗   Get rights and content ↗

● Full text access

Recommended articles

No articles found.

Highlights

- Temperature-dependent η-phase distribution is quantified through statistical analytics.
- A temperature-mediated η-phase morphology control strategy is established.
- Plate-like η-phases boost tensile strength via dislocation hindering mechanism.

期刊首页

期刊分区

通过中国科学院文献情报中心-期刊分区表公众号小程序查询得到：

学位论文送审专家评阅结果证明：

专家1：

评阅结果

学号：22260209　　　　　　　　　　　　　　　姓名：金巨烽

论文题目：镍基变形高温合金GH4350组织和拉伸性能研究

英文题目：Study on Microstructure and Tensile Properties of Nickel-Based Wrought Superalloy GH4350

**** 　　　**** 　　　****

评阅意见

* 评阅意见： GH4350合金作为重要的高温紧固件材料使用温度为750℃，本文针对航空发动机对耐高温紧固件日益严苛的服役需求，通过"合金制备-组织调控-性能表征-变形机理分析"方法，开展优化熔炼、均匀化、变形加工及热处理工艺等一系列

* 不足之处及修改意见： 1、文中括号段落，建议用中文格式的" ()"，代替英文格式的括号()；
2、66页图中的工程应变曲线（虽然第二章强调了借鉴方法），由于去掉了屈服前的应力应变曲线，对后续深入分析可

* 总体评价： A（优秀）

* 评阅结果： 同意修改后直接答辩

专家2：

评阅结果

学号：22260209　　　　　　　　　　　　　　　姓名：金巨烽

论文题目：镍基变形高温合金GH4350组织和拉伸性能研究

英文题目：Study on Microstructure and Tensile Properties of Nickel-Based Wrought Superalloy GH4350

**** 　　　**** 　　　****

评阅意见

* 评阅意见： 本文针对航空发动机紧固件用镍基变形高温合金GH4350材料，通过热处理调控方法系统研究了不同"固溶-时效"热处理制度对合金显微组织的影响，并构建"合金制备工艺—微观组织调控—高温拉伸性能"三元协同优化模型，为GH4350合

* 不足之处及修改意见： 1、文中的图题描述过长，应简化，如图1.13等等；
2、图题中有几处描述不对，如图2.3中有三幅图，但描述中只有（a）和（b）；图3.2的图题翻译有误；图3.20中图题有

* 总体评价： A（优秀）

* 评阅结果： 同意答辩

专家 3：

评阅结果

学号: 22260209　　　　　　　　　　姓名: 金巨峰

论文题目: 镍基变形高温合金GH4350组织和拉伸性能研究

英文题目: Study on Microstructure and Tensile Properties of Nickel-Based Wrought Superalloy GH4350

****　　　****　　　****

评阅意见

* 评阅意见: 该学位论文围绕镍基变形高温合金 GH4350 的组织特征及其拉伸性能展开研究，具有较好的工程应用背景与研究价值。论文文献综述较为全面，结构合理，图表规范，实验数据翔实，分析与讨论较为深入，整体写作较为规范。但在文字表

* 不足之处及修改意见: 1. 主要结论不需要这么多点，可以凝练成3点左右;
2. 有些图偏大，需缩小尺寸

* 总体评价: A（优秀）

* 评阅结果: 同意修改后直接答辩

专家姓名	评阅时间	总体评价	评阅结果
***		A（优秀）	同意修改后直接答辩
***		A（优秀）	同意答辩
***		A（优秀）	同意修改后直接答辩

浙江大学

硕士专业学位论文

中文论文题目：镍基变形高温合金 GH4350 组织和拉伸性能研究

英文论文题目：Study on Microstructure and Tensile Properties of Nickel-Based Wrought Superalloy GH4350

申请人姓名：

校 内 导 师：

行 业 导 师：

专业学位类别： 材料与化工

专业学位领域： 材料工程

研 究 方 向： 镍基变形高温合金

培 养 类 型： 全日制非定向

所 在 学 院： 工程师学院

论文提交日期： 二〇二五年四月八日

目 录

摘 要

GH4350 是一种航空发动机紧固件用镍基变形高温合金，具备高抗拉强度、抗疲劳、抗应力松弛和耐腐蚀性，并具备较低的膨胀系数，因其综合性能优异，有望进一步提高使用温度至 800 ℃。该合金主要通过细晶强化、固溶强化以及 γ′相沉淀强化获得高强度，但在 γ′相析出的同时也会析出少量 η 相，该相在热处理过程中随"温度-时间"参数演变。拉伸性能是变形高温合金关键的力学性能之一，对于紧固件的安全服役具有重要意义，因此需要深入研究 GH4350 在 800 ℃拉伸性能及变形机制。由于 η 相的形成对合金性能具有双重影响，其形貌分布既可阻碍位错运动提升强度，也可能成为裂纹萌生源。因此，厘清 η 相的析出动力学并调控其析出分布特征成为优化 GH4350 合金800 ℃高温拉伸性能的关键科学问题。

本文以 GH4350 为研究目标，在均匀化热处理及变形加工的基础上，系统研究了不同"固溶-时效"热处理制度对合金显微组织的影响，并基于典型显微组织开展 800 ℃拉伸性能测试，揭示了显微组织与拉伸性能的关联机制，获得以下主要结论：

（1）1180 ℃/30 h 均匀化处理降低 GH4350 合金的枝晶偏析，消除铸态析出相。该均匀化工艺为后续开坯、热轧及冷轧变形提供了组织基础。

（2）再结晶行为分析表明，GH4350 合金的再结晶起始温度高于 1000 ℃。当固溶温度超过 η 相溶解温度时，通过调控固溶温度与时间，可实现 30 μm~500 μm 梯度晶粒组织的制备且无 η 相残留；采用低于 η 相溶解温度固溶可使晶粒细化至 14 μm，而结合预析出 η 相工艺可进一步细化至 12 μm，但会伴随 η 相残留量增加及晶粒尺寸均匀性下降。

（3）η 相析出动力学研究表明，其形貌呈现显著的时效温度依赖性。通过调节一次时效温度可诱导 η 相从晶界短棒状向晶界板片状转变，并在高温下形成晶内魏氏结构组织。进一步结合低温二次时效处理，可在维持 η 相板片形貌稳定的同时促进 γ′相强化析出，实现双相协同强化。

（4）裂纹扩展机制研究表明，短棒状和板片状 η 相均会诱发 γ′相贫乏区，导致局部软化，不能阻碍裂纹扩展；短棒状 η 相沿晶界平行分布，诱发沿晶开裂加速裂纹扩展，而板片状 η 相因与晶界呈倾角分布可增强裂纹扩展阻力，使 800 ℃抗拉强度提升

13%。

（5）板片状 η 相可增强晶界强度，促使变形向晶内转移。晶内变形机制表现为强耦合型位错对剪切、层错剪切与奥罗万绕过机制的协同作用。

（6）当晶粒从 70 μm 细化至 30 μm 时，Hall-Petch 强化效应使屈服强度提升，同时单位晶界变形量降低促使校正断后伸长率增加，且板片状 η 相的裂纹阻碍能力未显著衰减，抗拉强度保持稳定；而晶粒进一步细化至 14 μm 时，晶界数量激增导致晶界滑动加剧，Hall-Petch 强化失效，同时 η 相形态由板片状退化为短棒状，裂纹扩展阻力下降，二者耦合作用致使屈服强度和抗拉强度同步降低，但单位晶界变形进一步减少使校正断后伸长率显著提升。

关 键 词：紧固件用镍基变形高温合金；晶粒尺寸；时效热处理；η 相；拉伸性能；变形机理

ABSTRACT

GH4350 is a nickel-based wrought superalloy for fasteners, characterized by high tensile strength, fatigue resistance, stress relaxation resistance, and corrosion resistance, coupled with a low thermal expansion coefficient. Its superior comprehensive properties make it promising for elevated temperature applications up to 800 °C. The alloy primarily achieves high strength through grain refinement strengthening, solid solution strengthening, and γ' phase precipitation strengthening. However, minor η phase precipitation accompanies γ' phase formation during heat treatment, with its evolution governed by temperature-time parameters. Tensile properties constitute one of the critical mechanical characteristics for wrought superalloys, bearing significant implications for the safe service of fasteners. This necessitates in-depth investigation into the tensile properties and deformation mechanisms of GH4350 at 800 °C. The η phase exhibits dual effects on alloy performance: while its morphological distribution can enhance strength by impeding dislocation motion, it may also serve as crack initiation sites. Consequently, elucidating the precipitation kinetics of η phase and precisely controlling its distribution characteristics emerge as the key scientific challenges for optimizing the high-temperature tensile performance of GH4350 alloy at 800 °C.

This study focuses on self-melted GH4350 and systematically investigates the effects of different "solution-aging" heat treatment regimes on the alloy's microstructure after homogenization heat treatment and deformation processing. Based on typical microstructures, tensile tests at 800 °C were conducted to reveal the correlation mechanism between microstructure and tensile properties. The main conclusions are as follows:

(1) Through duplex-melting and homogenization treatment at 1180 °C for 30 h, dendritic segregation and as-cast precipitates in GH4350 alloy are effectively eliminated. This homogenization process provides a microstructural foundation for subsequent forging, hot rolling, and cold rolling.

(2) Recrystallization behavior analysis indicates that the recrystallization onset temperature of GH4350 exceeds 1000 °C. When the solution treatment temperature exceeds the dissolution temperature of the η phase, gradient grain structures ranging from 30 μm to 500 μm are obtained without residual η phase by adjusting the solution temperature and time. Solution treatment below the dissolution temperature refines grains to 14 μm, while pre-precipitation of the η phase further reduces grain size to 12 μm. However, this process increases the residual η phase content and decreases grain size uniformity.

(3) The precipitation kinetics of the η-phase exhibit significant dependence on aging temperature. By adjusting the primary aging temperature, the η-phase morphology transitions from short rod-like at grain boundaries to plate-like structures, eventually forming an intragranular Widmanstätten structure at high temperatures. Further application of low-temperature secondary aging can stabilize the plate-like η-phase morphology while promoting the strengthening precipitation of γ', achieving dual-phase synergistic strengthening.

(4) The crack propagation mechanism study reveals that both short rod-like and plate-like η phases induce γ′ phase free zones, leading to local softening and failing to hinder crack propagation. Short rod-like η phase aligned along grain boundaries accelerates intergranular cracking, while plate-like η angled to grain boundaries enhances crack resistance, boosting 800°C tensile strength by 13%.

(5) Plate-like η-phase strengthens grain boundaries, promoting deformation transfer to the grain interior. The intragranular deformation mechanism exhibits a strong coupling effect among dislocation pair shearing, stacking fault shearing, and the Orowan bypass mechanism.

(6) Refining grain size from 70 μm to 30 μm boosts yield strength by nearly 10% via the Hall-Petch effect, while reduced deformation per grain boundary increases calibrated elongation. Plate-like η phases retain crack-blocking ability, maintaining ultimate tensile strength. Further refinement to 14 μm increases grain boundary density, intensifying sliding and negating Hall-Petch strengthening. Concurrent η phase degeneration to short rods reduces crack resistance, lowering both yield and ultimate tensile strengths, though further reduced deformation per grain boundary sharply improves calibrated elongation.

KEY WORDS: Nickel-based wrought superalloy; fasteners; grain size; aging heat treatment; η phase; tensile properties; deformation mechanism

第五章 结论与展望

5.1 总结

本文以镍基变形高温合金 GH4350 为研究对象，利用自主双联冶炼、均匀化热处理及变形加工，制备了合金样品，通过热处理调控系统研究了不同"固溶-时效"热处理制度对合金显微组织的影响，并基于典型显微组织开展 800 ℃拉伸性能测试，揭示了显微组织与拉伸性能的关联机制，获得以下主要结论：

（1）采用 1180 ℃/30 h 均匀化处理可有效消除 GH4350 合金枝晶偏析及铸态析出相，为后续开坯、热轧和冷轧加工提供了良好的组织基础。

（2）GH4350 的再结晶温度高于 1000 ℃。当固溶温度超过 η 相溶解温度时，通过调控固溶温度与时间可获得 30 μm~500 μm 的梯度晶粒组织且无 η 相残留；采用低于 η 相溶解温度固溶可将晶粒细化至 14 μm；结合预析出 η 相与低于 η 相溶解温度固溶工艺可进一步细化晶粒至 12 μm，但会导致 η 相残留量增加及晶粒尺寸均匀性降低。

（3）η 相析出形貌呈现显著的温度依赖性。通过调控一次时效温度可实现 η 相从晶界短棒状到晶界板片状到晶内魏氏组织的演变。结合低温二次时效处理可在维持 η 相形貌稳定的前提下促进 γ′相强化析出，实现 η 相与 γ′相的协同调控。

（4）短棒状与板片状 η 相均易引发裂纹萌生，并形成 γ′ PFZ，引起局部软化，不能阻碍裂纹扩展，但短棒状 η 相沿晶界平行分布会加速裂纹扩展，而板片状 η 相与晶界呈一定角度分布通可提升裂纹扩展阻力，使 A3 热处理试样的抗拉强度较 A1/A2 提升 13%。

（5）A3 热处理形成的板片状 η 相可增强晶界强度，促使变形向晶内转移。晶内变形机制表现为 SCD 型位错对剪切、SF 剪切与奥罗万绕过机制的协同作用。

（6）当时效工艺相同时，晶粒尺寸从 70 μm 细化至 30 μm 时，单位晶界变形量降低，塑性提升，在 Hall-Petch 效应的作用下，屈服强度增加且抗拉强度因板片状 η 相维持裂纹阻碍作用而保持稳定；进一步细化至 14 μm 后，单位晶界变形进一步减少使得塑性显著提升，但晶粒尺寸低于临界值导致细晶强化失效，同时 η 相退化为短棒状削弱裂纹阻碍能力，二者耦合作用致使屈服强度和抗拉强度均下降。

5.2 展望

本文研究了镍基变形高温合金 GH4350 热处理工艺对显微组织的影响，通过典型微观组织的 800 ℃拉伸性能测试初步揭示了组织-性能关联机制。研究结果可为该合金在 800 ℃服役条件下的高温拉伸性能优化提供组织设计指导。然而，显微组织演化涉及复杂相变过程，其精准调控与变形机理仍需深入探索，且需拓展至其他关键力学性能研究以实现合金综合性能优化。基于此，建议后续工作聚焦以下方向：

（1）基于预析出 η 相的细晶制备技术，系统研究预析出热处理工艺、变形工艺与固溶制度的交互作用机制，建立多工序协同调控模型，实现晶粒细化与均匀化。

（2）开展原位时效热处理研究，揭示 η 相从低温时效到高温时效过程中的形核与生长动力学，指导精准时效工艺设计。

（3）对不同晶粒尺寸样品的时效热处理制度进行针对性设计，获得该晶粒尺寸下最优的 γ'/η 相两相组织，进一步优化性能。开展原位拉伸测试，为探究裂纹萌生和扩展与不同形貌 η 相真实的关联关系提供更加有力的证据。

（4）开展长时高温持久和蠕变的研究，建立对应的热处理工艺-显微组织-变形机理的关联关系。开展紧固件的关键性能应力松弛和力学性能缺口敏感性的研究，并建立对应的热处理工艺-显微组织-变形机理的关联关系。